Zero-temperature localization in a sub-Ohmic spin-boson model investigated by an extended hierarchy equation of motion

Chenru Duan,[1] Zhoufei Tang,[1] Jianshu Cao,[2] and Jianlan Wu[1,*]
[1]*Physics Department, Zhejiang University, Hangzhou, Zhejiang 310027, China*
[2]*Department of Chemistry, Massachusetts Institute of Technology, Cambridge, Massachusetts 02139, USA*
(Received 24 January 2017; revised manuscript received 7 June 2017; published 28 June 2017)

With a decomposition scheme for the bath correlation function, the hierarchy equation of motion (HEOM) is extended to the zero-temperature sub-Ohmic spin-boson model, providing a numerically accurate prediction of quantum dynamics. As a dynamic approach, the extended HEOM determines the delocalized-localized (DL) phase transition from the extracted rate kernel and the coherent-incoherent dynamic transition from the short-time oscillation. As the bosonic bath approaches from the strong to weak sub-Ohmic regimes, a crossover behavior is identified for the critical Kondo parameter of the DL transition, accompanied by the transition from the coherent to incoherent dynamics in the localization.

DOI: 10.1103/PhysRevB.95.214308

I. INTRODUCTION

A spin-half particle embedded in a bosonic bath is a fundamental model system to understand many relevant topics in physics and chemistry, such as decoherence of a qubit and energy and electron transfer [1]. Despite a simple formulation, the spin-boson model (SBM) can explore rich phenomena of quantum dissipation. For an unbiased spin system coupled to a sub-Ohmic or Ohmic bath at zero temperature, a delocalized-localized (DL) phase transition occurs as the system-bath interaction increases [1]. The symmetry between the two degenerate spin states is broken and the population is localized at one of the spin states, which corresponds to the quantum phase transition in condensed matter [2,3].

Despite the difficulty of treating the bosonic bath exactly, especially under a strong system-bath interaction, the DL transition in the SBM has been studied through different approaches. The numerical renormalization group [4], quantum Monte Carlo (QMC) [5], and sparse polynomial space representation [6] have been used to generate numerically accurate predictions of the DL transition from the standpoint of quantum equilibrium and investigate the critical behavior. The variational polaron antasz and its extensions provide a mean-field picture of understanding the DL transition [7–11]. In particular, an analytical expression of the critical Kondo parameter is obtained in the strong sub-Ohmic regime [8]. The DL transition has also been investigated by dynamic approaches. The multilayer multiconfiguration time-dependent Hartree (ML-MCTDH) approach has explored in detail the dependence of the DL transition on control parameters [12,13]. By mapping a continuously distributed bosonic bath onto a one-dimensional chain of harmonic oscillators, the time-dependent density matrix renormalization group and variational matrix product state approach with optimized boson basis can efficiently calculate quantum dynamics of the SBM besides equilibrium properties [14–17]. In addition to the DL transition, the persistent coherence in the localized phase under a strong sub-Ohmic bath and the coherent-incoherent (CI) dynamic transition have attracted much attention [12,13,18–21]. The quantification of the interplay between the CI dynamic transition and the DL phase transition remains an important question.

Compared to other dynamic approaches, the hierarchy equation of motion (HEOM) solves quantum dissipative dynamics with the facilitation of auxiliary fields [22–28]. With great success in many problems, the HEOM was originally built on the assumption of an exponentially decaying bath correlation function $C(t)$, which is exact only for a few spectral densities $J(\omega)$. Numerical techniques, such as the Meier-Tannor decompositions of the spectral density and various expansion schemes of the Bose function, are introduced to expand the application of the HEOM [29–32]. The hybrid with a classical stochastic noise is applied to two special spectral densities at zero temperature [33,34]. However, the HEOM with these numerical improvements still has difficulty in dealing with bath correlation functions with a power-law tail. In a recent paper, we introduced the concept of the complete basis set to directly decompose $C(t)$ instead of $J(\omega)$ [35,36]. An extended HEOM, formally rigorous for a general bath, is constructed within a finite time range. The dynamics of the sub-Ohmic SBM is predicted by the extended HEOM, but the low efficiency of expanding $C(t)$ limits our study without identifying the DL transition.

In this paper, we introduce an approximate approach to decompose $C(t)$ and develop an extended HEOM valid for the bath correlation function with a power-law tail. The calculation of the extended HEOM determines the DL and CI transitions from the standpoint of dynamics. Our analysis identifies a crossover in the DL transition, which is correlated with the transition from the coherent to incoherent dynamics in the localized phase.

II. EXTENDED HIERARCHY EQUATION OF MOTION

A. Spin-boson model

The total Hamiltonian of an unbiased spin-boson model is given by [1]

$$H = \Delta\sigma_x + \frac{1}{2}\sum_j \left(p_j^2 + w_j^2 q_j^2\right) + \sigma_z \sum_j c_j q_j. \qquad (1)$$

*jianlanwu@zju.edu.cn

Throughout this paper, the reduced Planck constant $\hbar$ is treated as a unity. For the spin system, σ_x and σ_z are two Pauli matrices, and Δ is the tunneling amplitude between two degenerate spin states. For each jth harmonic oscillator of the environment, ω_j, p_j, and q_j are its oscillation frequency, momentum, and position, respectively. The system-bath interaction follows a bilinear form with c_j the coupling coefficient. The bath influence is characterized by a spectral density, $J(\omega) = (\pi/2)\sum_j (c_j^2/\omega_j)\delta(\omega-\omega_j)$, which follows a power-law dependence, $J(\omega) \sim \omega^s$, at low frequencies. The bosonic bath is categorized as Ohmic ($s = 1$), sub-Ohmic ($0 < s < 1$), and super-Ohmic ($s > 1$) [1]. With a cutoff function $f(\omega/\omega_c)$, the spectral density is written in a continuous form as

$$J(\omega) = \Theta(\omega)(\pi/2)\alpha\omega^s\omega_c^{1-s} f(\omega/\omega_c), \tag{2}$$

where $\Theta(\omega)$ is the Heaviside step function, α is the Kondo parameter describing the average system-bath interaction, and ω_c is the cutoff frequency. In this paper, we consider an exponential cutoff function, $f(\omega/\omega_c) = \exp(-\omega/\omega_c)$, and limit our investigation for the sub-Ohmic bath in the regime of $\omega_c \gg \Delta$.

B. Decomposition of the bath correlation function

Based on the spectral density, the bath time-correlation function is subsequently defined as

$$C(t) = \frac{1}{\pi}\int_0^\infty J(\omega)\left[\coth\frac{\beta\omega}{2}\cos\omega t - i\sin\omega t\right]d\omega, \tag{3}$$

where $\beta = 1/k_B T$ is the inverse product of temperature T and the Boltzmann constant k_B. Compared with the spectral density, the bath correlation function is directly required in the HEOM, so that we focus on the decomposition of $C(t) = C_{\rm R}(t) + iC_{\rm I}(t)$, where $C_{\rm R}(t)$ and $C_{\rm I}(t)$ are the real and imaginary parts, respectively. For a zero-temperature sub-Ohmic bath, $C(t)$ is analytically solved, including a short-time underdamped oscillation and a power-law decay, $C(t) \sim -(t\omega_c)^{-(1+s)}$, in the long-time limit. For a large but finite time range ($0 < t < t_{\rm max}$ and $t_{\rm max}\omega_c \gg 1$), we can introduce a complete set of orthonormal functions, such as the harmonic oscillator wave functions and discrete Fourier series, to simultaneously decompose $C_{\rm R}(t)$ and $C_{\rm I}(t)$ [33,35]. Due to a large number of basis functions for convergence, the follow-up extended HEOM is however limited to a small order of the hierarchic expansion [35].

Instead, we apply an incomplete set of oscillatory and nonoscillatory exponentially decaying functions for an approximate decomposition,

$$C_X^{\rm fit}(t) = a_{X;1}\cos(\omega_X t)e^{-\gamma_X t} + a_{X;2}\sin(\omega_X t)e^{-\gamma_X t} + \sum_{n=3}^{N_X} a_{X;n}e^{-\Gamma_{X;n-2}t}. \tag{4}$$

The fitting parameters, $\{a_{X;n},\omega_X,\gamma_X,\Gamma_{X;n}\}$, are allowed to be uncorrelated for the real ($X = {\rm R}$) and imaginary ($X = {\rm I}$) parts. The numbers of basis functions, $N_{\rm R}$ and $N_{\rm I}$, are also allowed to be different, which can help improve the numerical efficiency of the extended HEOM. In this decomposition scheme, two

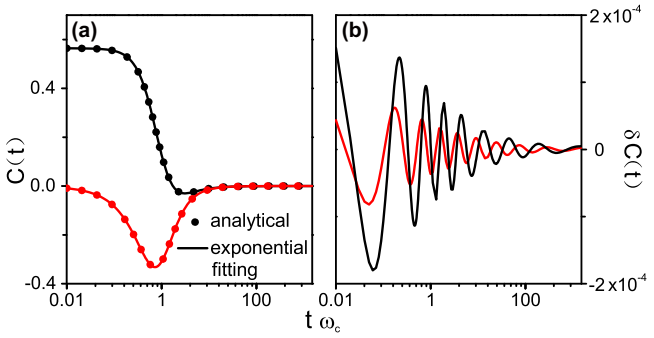

FIG. 1. The bath correlation function of a zero-T sub-Ohmic bath ($s = 0.5$). The black and red colors refer to the real and imaginary parts, respectively. (a) The solid lines are the results of the exponential fitting from Eq. (4), while the solid circles are the analytical results. (b) The numerical errors of the exponential fitting with $\delta C_X(t) = C_X^{\rm fit}(t) - C_X(t)$ ($X = {\rm R,I}$).

oscillatory terms reflect the short-time underdamped oscillation, while $N_X - 2$ nonoscillatory terms simulate the effective behavior of the power-law decay within different time ranges. The least-squares method, $\int_0^{t_{\rm max}}[C_X^{\rm fit}(t) - C_X(t)]^2 dt < \xi_X$, with bound constraints is applied to fit the real and imaginary parts separately. In the fitting process, we set the initial values of $\{\omega_X,\gamma_X\}$ from the short-time behavior of $C_X(t)$, and those of $\{\Gamma_{X;n}\}$ from the integrals of $C_X(t)$ over specified time ranges. The convergence of the fitting parameters is robust against a reasonable variation of the initial values. For the example of $s = 0.5$ and $t_{\rm max}\omega_c = 1500$ in Fig. 1, a numerically good fitting result of $N_R = 7$ and $N_I = 9$ is obtained for $C_{\rm R}(t)$ and $C_{\rm I}(t)$, giving $\xi_{\rm R} = 5.6\times10^{-8}$ and $\xi_{\rm I} = 1.3\times10^{-8}$. As shown in Fig. 1(b), the numerical error of $C^{\rm fit}(t)$ is considerably small ($<2\times10^{-4}$) for $0 < t < t_{\rm max}$. Therefore, the numerical acceptance of $C^{\rm fit}(t)$ allows us to perform the extended HEOM with a significantly improved efficiency.

C. Extended HEOM

The HEOM is a theoretical method of quantum dynamics built on a complete dynamic set consisting of the reduced density matrix (RDM) and its auxiliary fields [22,35]. Here we briefly introduce the structure of the extended HEOM while a simplified derivation is provided in Appendix A. In our previous work [35], the bath correlation function is expanded over a complete set of orthonormal functions, $C(t) = \sum_n (a_n + ib_n)\varphi_n(t)$, which is formally exact for a bath spectral density at any temperature. The auxiliary fields are constructed based on the chosen basis functions $\{\varphi_n(t)\}$ instead of $C(t)$. Our decomposition of the bath correlation function in Eq. (4) can be summarized into

$$C(t) \approx \sum_{n=1}^{N_{\rm R}} a_{{\rm R};n}\varphi_{{\rm R};n}(t) + i\sum_{m=1}^{N_{\rm I}} a_{{\rm I};m}\varphi_{{\rm I};m}(t). \tag{5}$$

The basis functions are oscillatory and nonoscillatory exponentially decaying functions, given by

$$\{\varphi_{X;n}(t)\} = \{\cos\omega_X t e^{-\gamma_X t}, \sin\omega_X t e^{-\gamma_X t}, e^{-\Gamma_{X;1}t}, \ldots\}, \tag{6}$$

with $X = \mathrm{R}$ and I. For the two separated basis sets, $\{\varphi_{\mathrm{R};n}(t)\}$ and $\{\varphi_{\mathrm{I};m}(t)\}$, the time-differential operator is transformed into two different matrices, $\partial_t \varphi_{\mathrm{R};n}(t) = \sum_{n'} \eta_{\mathrm{R};n,n'} \varphi_{\mathrm{R};n'}(t)$ and $\partial_t \varphi_{\mathrm{I};m}(t) = \sum_{m'} \eta_{\mathrm{I};m,m'} \varphi_{\mathrm{I};m'}(t)$.

An arbitrary auxiliary field on the $h(\geqslant 0)$th order is constructed as

$$\begin{aligned}\sigma_h^{\binom{n_1,\cdots,n_k}{m_1,\cdots,m_l}}(t) = \mathcal{U}_{\mathrm{S}}(t)\mathcal{T}_+\Big\{ &\int_0^t d\tau_1 \varphi_{\mathrm{R};n_1}(t-\tau_1)[-i\mathcal{L}_z(\tau_1)] \\ &\times \cdots \int_0^t d\tau_k \varphi_{\mathrm{R};n_k}(t-\tau_k)[-i\mathcal{L}_z(\tau_k)] \\ &\times \int_0^t d\tau_1' \varphi_{\mathrm{I};m_1}(t-\tau_1')\mathcal{S}_z(\tau_1') \\ &\times \cdots \int_0^t d\tau_l' \varphi_{\mathrm{I};m_l}(t-\tau_l')\mathcal{S}_z(\tau_l')\mathcal{U}_{\mathrm{RDM}}(t)\Big\}\rho_{\mathrm{S}}(0).\end{aligned} \tag{7}$$

Here $\mathcal{L}_z = [\sigma_z, \dots]$ and $\mathcal{S}_z = [\sigma_z, \dots]_+$ are the commutator and anticommutator of the Pauli σ_z matrix. For the unbiased SBM, the system time propagator of the density matrix is $\mathcal{U}_{\mathrm{S}}(t) = \exp(-i\Delta\mathcal{L}_x t)$, where $\mathcal{L}_x = [\sigma_x, \dots]$ is the commutator of the Pauli σ_x matrix. In addition, $\mathcal{U}_{\mathrm{RDM}}(t)$ is the time propagator for the reduced density matrix in the interaction picture. All the math symbols in the calligraphic font denote superoperators in the Liouville space. The auxiliary field $\sigma_h^{\binom{n_1,\cdots,n_k}{m_1,\cdots,m_l}}(t)$ defined in Eq. (7) is identified by the two sequences of indices, $(n_1, \dots, n_k)$ and $(m_1, \dots, m_l)$. Corresponding to the two basis sets, $\{\varphi_{\mathrm{R};n}(t)\}$ and $\{\varphi_{\mathrm{I};m}(t)\}$, each index represents a specific basis function, i.e., $1 \leqslant n_i \leqslant N_{\mathrm{R}}$ for $1 \leqslant i \leqslant k$ and $1 \leqslant m_j \leqslant N_{\mathrm{I}}$ for $1 \leqslant j \leqslant l$. To avoid overcounting, these indices are arranged in an incremental sequence, i.e.,

$$n_1 \leqslant n_2 \leqslant \cdots \leqslant n_k \ \text{ and } \ m_1 \leqslant m_2 \leqslant \cdots \leqslant m_l. \tag{8}$$

The total number of nonzero indices defines the order of the hierarchic expansion, i.e., $h = k + l$. On the lowest order ($h = 0$), the unique dynamic element recovers the RDM, i.e., $\sigma_0(t) = \rho_{\mathrm{S}}(t)$. More details of this construction can be found in Appendix A and Ref. [35].

Following a straightforward derivation demonstrated in Appendix A, we take the time derivative of Eq. (7) to obtain an extended HEOM as

$$\begin{aligned}\partial_t \sigma_h^{\binom{n_1,\cdots,n_k}{m_1,\cdots,m_l}}(t) = &-i\Delta\mathcal{L}_x \sigma_h^{\binom{n_1,\cdots,n_k}{m_1,\cdots,m_l}}(t) - i\mathcal{L}_z \sum_{j=1}^{k} \varphi_{\mathrm{R};n_j}(0)\sigma_{h-1}^{\binom{\cdots,n_{j-1},n_{j+1},\cdots}{\cdots}}(t) + \mathcal{S}_z \sum_{j=1}^{l} \varphi_{\mathrm{I};m_j}(0)\sigma_{h-1}^{\binom{\cdots}{\cdots,m_{j-1},m_{j+1},\cdots}}(t) \\ &+ \sum_{j=1}^{k}\sum_{j'=1}^{N_{\mathrm{R}}} \eta_{\mathrm{R};j,j'}\sigma_h^{\binom{\cdots,n_{j-1},n_{j'},n_{j+1},\cdots}{\cdots}}(t) + \sum_{j=1}^{l}\sum_{j'=1}^{N_{\mathrm{I}}} \eta_{\mathrm{I};j,j'}\sigma_h^{\binom{\cdots}{\cdots,m_{j-1},m_{j'},m_{j+1},\cdots}}(t) \\ &- i\mathcal{L}_z \sum_{n_{k+1}=1}^{N_{\mathrm{R}}} a_{\mathrm{R};n_{k+1}}\sigma_{h+1}^{\binom{\cdots,n_k,n_{k+1}}{\cdots}}(t) - i\mathcal{L}_z \sum_{m_{l+1}=1}^{N_{\mathrm{I}}} a_{\mathrm{I};m_{l+1}}\sigma_{h+1}^{\binom{\cdots}{\cdots,m_l,m_{l+1}}}(t).\end{aligned} \tag{9}$$

Notice that Eq. (9) can recover a standard HEOM form if the two expansion basis sets are merged into a single set and the oscillatory exponentially decaying functions are reexpressed using complex decay rates. To illustrate the physical picture behind our decomposition scheme and allow the possibility of nonexponential expansion functions, we will present our extended HEOM in a general form as shown in Eq. (9).

D. Numerical comparison with the ML-MCTDH

To verify the numerical reliability of the extended HEOM in Eqs. (4)–(9), we calculate the quantum dynamics of the zero-temperature SBM with a sub-Ohmic spectral density, which was rarely discussed in previous HEOM studies. In our calculation, Eq. (9) is truncated at a certain order of the hierarchic expansion, H. With small expansion numbers, e.g., $N_{\mathrm{R}} = 7$ and $N_{\mathrm{I}} = 9$, from the exponential fitting, we extend the order of the hierarchic expansion up to $H = 14$. For simplicity, we assume a system-bath factorized initial condition with the entire population at the spin-up state. A more general treatment for a system-bath entangled initial state may require the HEOM of an imaginary time [23,36].

In Fig. 2, we present the converged results of the spin population difference (equivalent to the average magnetic moment), $\langle\sigma_z(t)\rangle = \mathrm{Tr}\{\sigma_z\rho_{\mathrm{S}}(t)\}$, for six parameter sets of the spectral exponent s, Kondo parameter α, and cutoff frequency ω_c. The dynamics with the same parameter sets were calculated previously by a numerically accurate method, the ML-MCTDH [13]. The numerical comparison in Fig. 2 confirms an excellent agreement between the predictions of the extended HEOM and the ML-MCTDH over the whole time range calculated.

The numerical error of our extended HEOM is mainly limited by the fitting error of the bath correlation function if a convergent hierarchic expansion order is reached. The decomposition of $C(t)$ in Eq. (4) is under an assumption of a finite time range ($0 < t < t_{\max}$) so that the prediction of the extended HEOM is valid for $t < t_0$, where the new upper limit t_0 is roughly smaller than $t_{\max}$. However, the long-time steady state can still be probed reliably if t_0 is large enough. For example, most of the numerical calculations in the next section are based on an upper limit of $t_0 \approx 60\Delta^{-1}$ under the condition of $\omega_c/\Delta = 20$ and $t_{\max} = 1500\omega_c^{-1}$. The value of t_0 is much larger than the intrinsic time scale of the spin system ($\sim\Delta^{-1}$).

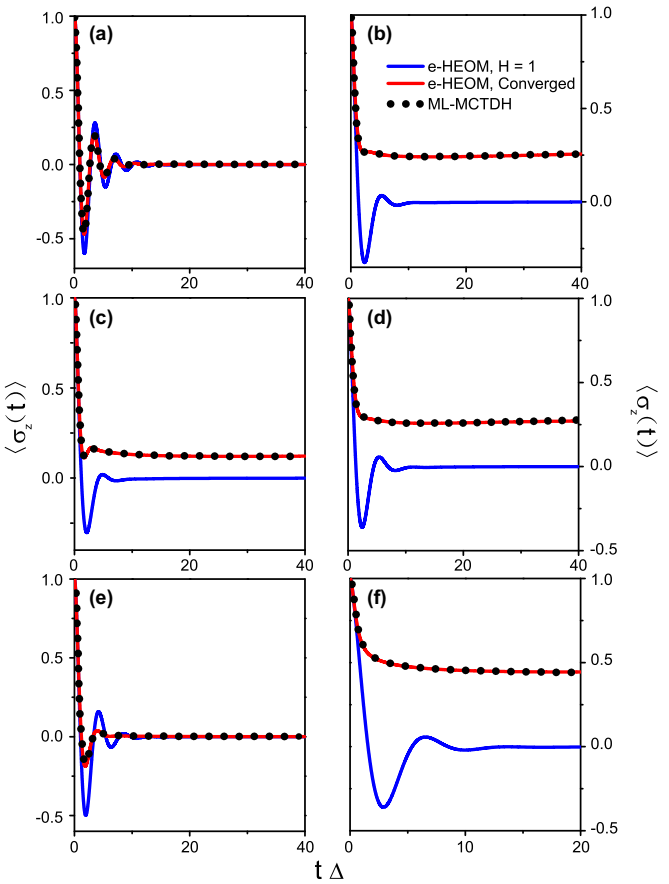

FIG. 2. The time evolution of $\langle\sigma_z(t)\rangle$ for the zero-T sub-Ohmic SBM with six different sets of parameters: (a) $\{\alpha = 0.05, s = 0.5, \omega_c/\Delta = 20\}$, (b) $\{\alpha = 0.15, s = 0.5, \omega_c/\Delta = 20\}$, (c) $\{\alpha = 0.2, s = 0.5, \omega_c/\Delta = 10\}$, (d) $\{\alpha = 0.1, s = 0.5, \omega_c/\Delta = 40\}$, (e) $\{\alpha = 0.2, s = 0.75, \omega_c/\Delta = 10\}$, and (f) $\{\alpha = 0.5, s = 0.75, \omega_c/\Delta = 10\}$. The blue and red solid lines are the first-order ($H = 1$) and converged results of the extended HEOM. The solid circles are the previous results of the ML-MCTDH [13].

III. APPLICATION OF THE EXTENDED HEOM TO THE ZERO-TEMPERATURE SPIN-BOSON MODEL

A. Delocalized-localized phase transition

Figure 3(a) presents our HEOM results of zero-temperature $\langle\sigma_z(t)\rangle$ using $\{s = 0.5, \omega_c/\Delta = 20\}$ for a series of Kondo parameters, $0.02 \leqslant \alpha \leqslant 0.15$. As α increases, $\langle\sigma_z(t)\rangle$ deviates from zero in the long time. Under a normal circumstance, the population is evenly distributed in the two spin states, i.e., $\langle\sigma_z(t \to \infty)\rangle = 0$, due to the degeneracy in their energy levels. However, large quantum fluctuations of the bath induce a symmetry breaking at zero temperature and more population is localized at the initial spin state, i.e., $\langle\sigma_z(t \to \infty)\rangle \neq 0$. This DL transition is a pure quantum phenomenon since no thermal fluctuations exist at zero temperature [1,2].

A key step of understanding the DL transition is to identify the critical point α_c and draw a phase diagram. Although the localization is observed from the time evolution of $\langle\sigma_z(t)\rangle$, it is difficult to obtain the critical Kondo parameter α_c directly from quantum dynamics since $\langle\sigma_z(t > t_0)\rangle$ is not determined exactly. Here we compress the extended HEOM into a time-convoluted equation for $\langle\sigma_z(t)\rangle$, which reads

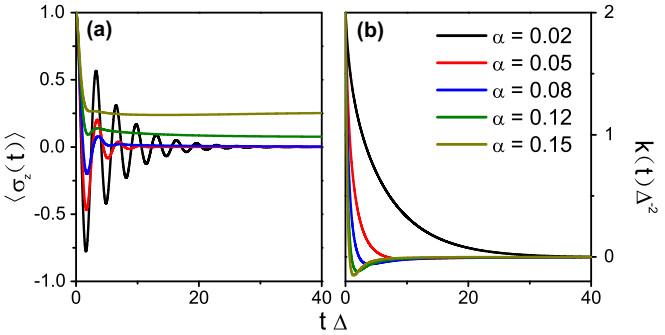

FIG. 3. (a) The time evolution of $\langle\sigma_z(t)\rangle$ predicted by the extended HEOM for $s = 0.5$ and $\omega_c/\Delta = 20$. From bottom to top, the lines correspond to $\alpha = 0.02$ (black), 0.05 (red), 0.08 (blue), 0.12 (green), and 0.15 (dark yellow). (b) The rate kernel $k(t)$ for each value of α in (a) is plotted and labeled with the same color.

$$d_t\langle\sigma_z(t)\rangle = -2\int_0^t k(t-\tau)\langle\sigma_z(\tau)\rangle d\tau. \tag{10}$$

Based on the numerical result of $\langle\sigma_z(t)\rangle$, the rate kernel $k(t)$ is extracted from Eq. (10) by discretizing the time-differential and time convolution. The time scale of $k(t)$ is often smaller than that of $\rho_S(t)$, which can be used to implement the transfer tensor method [37]. The results of $k(t)$ for the same sets of $\{s, \omega_c/\Delta, \alpha\}$ in Fig. 3(a) are provided in Fig. 3(b). For $\alpha = 0.02$, the rate kernel $k(t)$ decays slowly with time and almost stays positive. With the increase of α, the initial decay of $k(t)$ is accelerated. After certain time, a large negative rate kernel appears, which can be viewed as a mechanism to freeze the population transfer process.

Next we apply the Laplace transform, $\tilde{g}(z) = \int_0^\infty g(t)e^{-zt}dt$ with $g(t) = k(t)$ and $\langle\sigma_z(t)\rangle$. Equation (10) is changed to $\langle\tilde{\sigma}_z(z)\rangle = [z + 2\tilde{k}(z)]^{-1}\langle\sigma_z(0)\rangle$ in the Laplace z space. The DL transition arises from a singularity of $\langle\tilde{\sigma}_z(z)\rangle$ at $z = 0$ [1,19]. The symmetry of the two spin states is broken spontaneously, and the steady state is trapped in one of two poles. This singularity is induced when the zeroth-order moment, $\kappa_0 = \int_0^\infty k(t)dt$, vanishes. The critical Kondo parameter α_c is dynamically determined by the condition of $\kappa_0 = 0$. To numerically integrate the rate kernel, we separate $k(t)$ into a numerically accurate part ($t < t_0$) from the extended HEOM and a remaining long-time tail ($t > t_0$) from an approximate fitting $k^{\rm fit}(t)$ around t_0. For the example of $\{s = 0.5, \omega_c/\Delta = 20, \alpha = 0.12\}$, the separation point is $t_0 = 60\Delta^{-1}$ and an exponentially decaying function is used for the long-time tail [38]. The zeroth-order moment is estimated as

$$\kappa_0 = \int_0^{t_0} k(t)dt + \int_{t_0}^\infty k^{\rm fit}(t)dt. \tag{11}$$

In Fig. 4, the results with $\{s = 0.5, \omega_c/\Delta = 20\}$ show that κ_0 decreases quickly as the Kondo parameter α increases and is held around a small number for $\alpha \gtrsim 0.120$. The same behavior is observed for the results with $s = 0.4$ and 0.6. Due to the numerical error in the long-time tail $k^{\rm fit}(t)$, a small uncertainty is expected in the numerical estimation of κ_0. A numerical range is considered in the estimation of the critical point α_c.

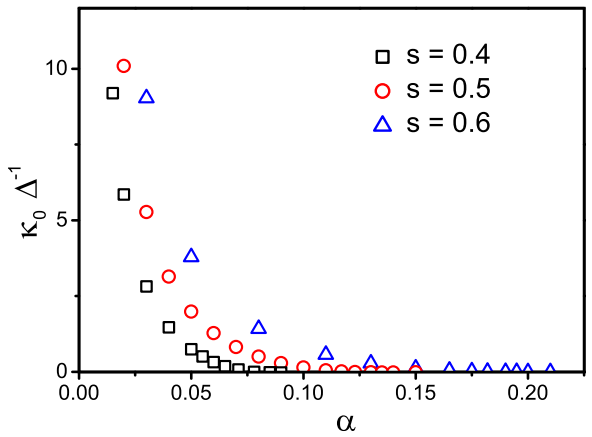

FIG. 4. For $\omega_c/\Delta = 20$, the change of the zeroth-order moment, $\kappa_0 = \int_0^\infty k(t)dt$, with the Kondo parameter α under three spectral exponents, $s = 0.4$ (squares), 0.5 (circles), and 0.6 (triangles).

The lower bound arises from the condition that κ_0 first reaches its numerical uncertainty, e.g., $\kappa_0 \approx 0.01\Delta$ for $s = 0.5$. The upper bound is determined as κ_0 drops to zero. For $s = 0.5$ and $\omega_c/\Delta = 20$, the critical point of the DL phase transition is estimated as $0.119 < \alpha_c < 0.123$.

Figure 5 presents the result of α_c for $0.30 \leqslant s \leqslant 0.90$ with $\omega_c/\Delta = 20$. The critical Kondo parameter α_c monotonically increases with the spectral exponent s. The delocalized and localized phases are below and above the transition line of $\alpha_c(s)$, respectively. Here we compare with a previous result of the QMC based on a sudden cutoff in the spectral density, i.e., $f(\omega/\omega_c \leqslant 1) = 1$ and $f(\omega/\omega_c > 1) = 0$ [5]. As shown in Fig. 5(a), our phase diagram is consistent with the predictions of the equilibrium methods [4–6]. The discrepancy is due to the difference of $f(\omega/\omega_c)$. In Ref. [8], a generalized polaron ansatz is used to derive an analytical expression of α_c for $0 < s < 0.5$ and $\omega_c/\Delta \to \infty$. Here we consider the limit of

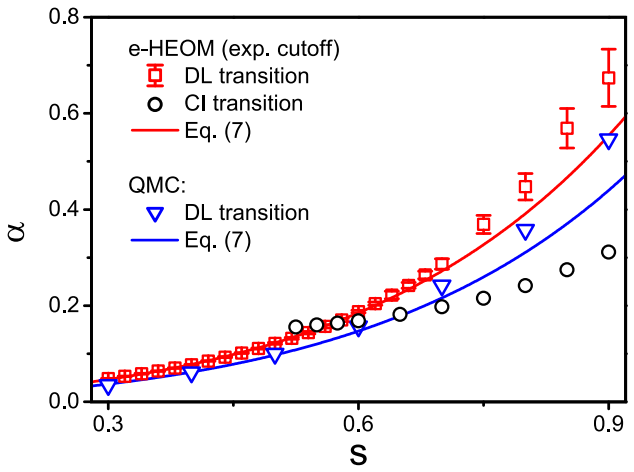

FIG. 5. The phase diagram of the zero-T sub-Ohmic SBM ($\omega_c/\Delta = 20$). The red squares with error bars are the results of α_c from the extended HEOM, and the red line is the fitting result from Eq. (12). The black circles are the results of $\alpha_{\rm CI}$. As a comparison, the result of α_c from the QMC [5] is shown in blue triangles, together with a blue line for its fitting result from Eq. (12).

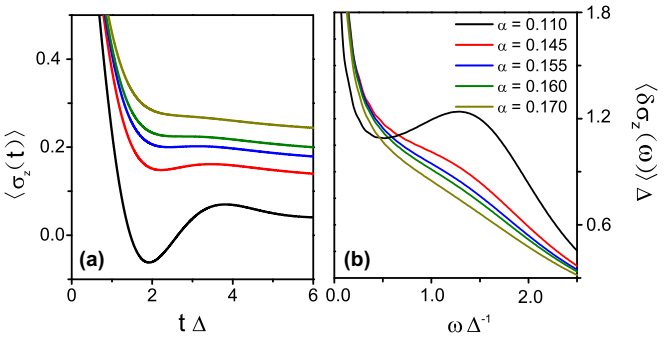

FIG. 6. (a) The short-time evolution of $\langle\sigma_z(t)\rangle$ for $s = 0.55$ and $\omega_c/\Delta = 20$. From bottom to top, the lines correspond to $\alpha = 0.11$ (black), 0.145 (red), 0.155 (blue), 0.16 (green), and 0.17 (dark yellow). (b) The Fourier transform $\langle\delta\sigma_z(\omega)\rangle$ for each α in (a) is plotted and labeled with the same color.

$s \to 0$ and take its asymptotic form,

$$\alpha_c \approx cs(2\Delta/\omega_c)^{1-s}. \tag{12}$$

Instead of a fixed number of $c = 1/2$ from the mean-field prediction [8], the prefactor c is allowed to be a free fitting parameter (see Appendix B). Equation (12) with $c = 0.775$ quantitatively describes α_c over a broad range of $s \leqslant 0.6$, beyond the mean-field prediction (see Fig. 5). The same behavior is observed for the result of the QMC, where the prefactor is changed to $c = 0.616$. The linear to nonlinear change in $\alpha_c \times (2\Delta/\omega_c)^{s-1}$ defines a crossover behavior of the DL transition as the bath approaches from the strong to weak sub-Ohmic regimes.

B. Coherent-incoherent dynamic transition

In addition to the DL phase transition in the long-time steady state, the short-time dynamics is also strongly affected by the system-bath interaction. In Fig. 6(a), we present the short-time evolution of $\langle\sigma_z(t)\rangle$ for $s = 0.55$ and $\omega_c/\Delta = 20$. For a small Kondo parameter (e.g., $\alpha = 0.11$), an underdamped oscillation is observed, which indicates a coherent motion. With the increase of α, the screening effect of the environment is strengthened and the oscillation of $\langle\sigma_z(t)\rangle$ is weakened. For $\alpha \geqslant 0.160$, $\langle\sigma_z(t)\rangle$ monotonically decays with time so that the motion becomes incoherent. A CI dynamic transition thus occurs at the Kondo parameter of $\alpha_{\rm CI} \approx 0.160$ for $s = 0.55$ and $\omega_c/\Delta = 20$. The transition parameter $\alpha_{\rm CI}$ can be alternatively estimated using the Fourier transform,

$$\langle\delta\sigma_z(\omega)\rangle = 2\int_0^\infty \langle\delta\sigma_z(t)\rangle\cos(\omega t)dt \tag{13}$$

with $\langle\delta\sigma_z(t)\rangle = \langle\sigma_z(t)\rangle - \langle\sigma_z(t\to\infty)\rangle$. In practice, the upper limit of the integration in Eq. (13) is set to be t_0 (i.e., $\int_0^\infty \to \int_0^{t_0}$), and the long-time steady state is approximated as $\langle\sigma_z(t\to\infty)\rangle \approx \langle\sigma_z(t_0)\rangle$. These two approximations are acceptable since we focus on the short-time evolution of $\langle\sigma_z(t)\rangle$. As shown in Fig. 6(b), the coherent motion of $\langle\sigma_z(t)\rangle$ leads to a side peak of $\langle\delta\sigma_z(\omega)\rangle$ centered at a nonzero frequency which is less than 2Δ due to the screening effect of the bath. This side peak is weakened with the increase of α and eventually disappears at $\alpha_{\rm CI} \approx 0.160$. Thus, the CI

dynamic transition is identified consistently from both time and frequency domains.

Next we calculate the CI transition parameter $\alpha_{\rm CI}$ as a function of the sub-Ohmic exponent s. Under the numerically converged regime of the extended HEOM, we always find an oscillated motion for the time evolution of $\langle\sigma_z(t)\rangle$ with $s \leqslant 0.5$. The CI dynamic transition only occurs for $s > 0.5$, and the numerical result of $\alpha_{\rm CI}(s > 0.5)$ is presented in Fig. 5 under the condition of $\omega_c/\Delta = 20$. It is interesting to point out that the CI transition line does not always lie below the DL transition line [21]. In particular, the CI dynamic transition occurs in the localized phase for $0.5 < s \lesssim 0.575$, while in the delocalized phase for $s \gtrsim 0.575$. Instead of $s = 0.5$, our numerical calculation suggests the crossing point of the DL and CI transition lines at $s \approx 0.575$. This difference may be attributed to a finite cutoff frequency, $\omega_c/\Delta \neq \infty$. In addition, this crossing point is close to the upper limit, $s \approx 0.6$, of the mean-field prediction in Eq. (12). This observation thereby suggests that the crossover behavior in the DL phase transition is accompanied by the transition from the coherent to incoherent localization as the bath becomes less sub-Ohmic and more Ohmic-like.

IV. SUMMARY

In summary, we extend the HEOM with a decomposition technique for the bath correlation function $C(t)$. A series of oscillatory and nonoscillatory exponentially decaying functions can efficiently simulate $C(t)$ with a slow-decaying tail. This approximate but reliable approach is based on a simple physical picture of separating a finite-time range into a series of time bins, each generating an effective exponential decay. As a result, an extended HEOM with greatly improved efficiency is constructed, but meanwhile the numerical accuracy is the same as that of the ML-MCTDH in predicting quantum dynamics. Our decomposition scheme can be employed to more complicated spectral densities at any environment temperature, which thus significantly expands the applicability of the HEOM. Additional studies will test its reliability in various problems.

In this paper, the extended HEOM is applied to the zero-T sub-Ohmic SBM. Based on dynamic results of the extended HEOM, we successfully observe the DL phase transition from the long-time evolution of the average magnetic moment $\langle\sigma_z(t)\rangle$. The critical point α_c is estimated using the zero integral of the rate kernel. The resulting DL phase diagram is consistent with previous results from the quantum equilibrium methods, although a different cutoff function of the spectral density was applied. Regarding an asymptotic relation, we identify a crossover behavior of the critical point around the sub-Ohmic exponent at $s \approx 0.6$, as the bosonic bath changes from the strong to weak sub-Ohmic regime. In addition, the short-time dynamics of $\langle\sigma_z(t)\rangle$ predicted by the extended HEOM allow us to identify the CI dynamic transition. The DL and CI transition lines cross with each other around $s \approx 0.575$, which is close to the crossover position $s \approx 0.6$ of the DL critical point. The dynamic crossover from the coherent to incoherent localization is thus accompanied. Overall, our HEOM calculation provides a quantitative description to understand the interplay between the DL and CI transitions.

ACKNOWLEDGMENTS

The work reported here is supported by the Ministry of Science and Technology of China (MOST-2014CB921203), the National Nature Science Foundation of China (NSFC-21573195), and the Fundamental Research Funds for the Central Universities in China.

APPENDIX A: DERIVATION OF THE EXTENDED HIERARCHY EQUATION OF MOTION

We briefly review the derivation of the extended HEOM, which follows closely the approach in Ref. [35]. To be consistent with the main text, we only consider the situation of an unbiased spin coupled with a bosonic bath. The derivation can be straightforwardly extended to an arbitrary quantum system.

The total Hamiltonian $H_{\rm tot}$ consists of three terms: the bare system Hamiltonian $H_{\rm S}$, the bare bath Hamiltonian $H_{\rm B}$, and their interaction $H_{\rm SB}$, i.e., $H_{\rm tot} = H_{\rm S} + H_{\rm B} + H_{\rm SB}$. Here the system Hamiltonian of an unbiased spin reads $H_{\rm S} = \Delta\sigma_x$, with σ_x the Pauli matrix and Δ the tunneling amplitude between the two spin states. The Hamiltonian of the bosonic bath reads $H_{\rm B} = (1/2)\sum_j (p_j^2 + \omega_j^2 q_j^2)$, where ω_j, p_j, and q_j are the frequency, momentum, and position of the jth harmonic oscillator. The system-bath interaction takes a bilinear form, $H_{\rm SB} = \sigma_z \sum_j c_j q_j$, which subsequently defines the bath spectral density, $J(\omega) = (\pi/2)\sum_j (c_j^2/\omega_j)\,\delta(\omega - \omega_j)$, and the bath correlation function, $C(t) = (1/\pi)\int_0^\infty J(\omega)[\coth(\beta\omega/2)\cos(\omega t) - i\sin(\omega t)]d\omega$.

To evaluate quantum dynamics of the spin system, we introduce the interaction picture of $H_0 = H_{\rm S} + H_{\rm B}$. The time evolution of the total density matrix $\rho_{\rm tot}^I(t)$ is governed by the Liouville equation,

$$\partial_t \rho_{\rm tot}^I(t) = -\mathcal{L}_{\rm SB}(t)\rho_{\rm tot}^I(t), \tag{A1}$$

where the superscript I denotes the interaction picture, and the commutator $\mathcal{L}_{\rm SB}(t) = [H_{\rm SB}(t), \dots]$ is treated as a Liouville superoperator. The time-dependent system-bath interaction, $H_{\rm SB}(t) = \sigma_z(t)F(t)$, includes two terms, $\sigma_z(t) = \exp(iH_{\rm S}t)\sigma_z\exp(-iH_{\rm S}t)$ and $F(t) = \exp(iH_{\rm B}t)\sum_j c_j q_j \exp(-iH_{\rm B}t)$. After the partial trace $\mathrm{Tr}_{\rm B}$ over the bath degrees of freedom, the reduced density matrix (RDM) of the spin system is given by $\rho_{\rm S}(t) = \mathrm{Tr}_{\rm B}\{\rho_{\rm tot}(t)\}$. The time integration of Eq. (1) leads to a formal solution of the RDM,

$$\rho_{\rm S}^I(t) = \mathrm{Tr}_{\rm B}\left\{\mathcal{T}_+ \exp\left[-i\int_0^t d\tau\,\mathcal{L}_{\rm SB}(\tau)\right]\rho_{\rm B}^{\rm eq}\right\}\rho_S(0), \tag{A2}$$

where $\mathcal{T}_+$ is the forward time-ordering operator. In Eq. (A2), we assume a system-bath factorized initial state with $\rho_{\rm tot}(0) = \rho_{\rm S}(0)\otimes\rho_{\rm B}^{\rm eq}$, where $\rho_{\rm B}^{\rm eq} \propto \exp(-\beta H_{\rm B})$ is the equilibrium distribution of an isolated bath. Although our derivation is based on the assumption of the factorized state, the (extended) HEOM can in principle be applied to other initial conditions. Due to the Gaussian property of the bosonic bath, the cumulant expansion is used to simplify Eq. (A2), giving

$$\rho_{\rm S}^I(t) = \mathcal{U}_{\rm RDM}(t)\rho_S(0), \tag{A3}$$

where the time propagator of the RDM is written in a time-ordered exponential form,

$$\mathcal{U}_{\rm RDM}(t) = \mathcal{T}_+ \exp\left[-\int_0^t \mathcal{W}(\tau)d\tau\right]. \tag{A4}$$

The transition rate kernel in Eq. (A4) is given by

$$\mathcal{W}(t) = \int_0^t d\tau \mathcal{L}_z(t)C_{\rm R}(t-\tau)\mathcal{L}_z(\tau) + i\mathcal{L}_z(t)C_{\rm I}(t-\tau)\mathcal{S}_z(\tau). \tag{A5}$$

In Eq. (A5), $C_{\rm R}(t)$ and $C_{\rm I}(t)$ are the real and imaginary parts of the bath correlation function, while $\mathcal{L}_z(t) = [\sigma_z(t), \dots]$ and $\mathcal{S}_z(t) = [\sigma_z(t), \dots]_+$ are the commutator and the anticommutator of σ_z in the interaction picture. The RDM in the Schrödinger picture is subsequently obtained after a unitary transformation, given by $\rho_{\rm S}(t) = \mathcal{U}_{\rm S}(t)\rho_{\rm S}^I(t) = \mathcal{U}_{\rm S}(t)\mathcal{U}_{\rm RDM}(t)\rho_S(0)$ with $\mathcal{U}_{\rm S}(t) = \exp(-i\mathcal{L}_{\rm S}t)$ and $\mathcal{L}_{\rm S} = [H_{\rm S}, \dots]$.

The (extended) HEOM is to solve the time derivative of the RDM with the facilitation of auxiliary fields. First, we provide the construction of a general auxiliary field. Since the bath correlation function can take an arbitrary form, a more systematic way is to decompose $C(t)$ using a set of basis functions $\{\varphi_j(t)\}$ so that the auxiliary field is built through $\{\varphi_j(t)\}$ instead of $C(t)$. In our previous paper [35], both $C_{\rm R}(t)$ and $C_{\rm I}(t)$ are decomposed over the same complete basis set, which is however unnecessary since these two terms are separated in the transition rate kernel $\mathcal{W}(t)$. Instead, we introduce the separated decompositions, $C_X(t) = \sum_j a_{X;j}\varphi_{X;j}(t)$, where $X = {\rm R,I}$ represents the real (R) and imaginary (I) parts, respectively. To preserve the formal accuracy, $\{\varphi_{X;j}(t)\}$ is required to be a complete basis set of orthonormal functions with $a_{X;j}$ the expanding coefficient. However, the incomplete basis sets such as the exponentially decaying functions in the main text can be numerically much more efficient although the decomposition is approximate. The discretized decomposition in general implies a finite time range, $0 < t < t_{\rm max}$, for the bath correlation function. An arbitrary auxiliary field is then defined as

$$\begin{aligned}\sigma_h^{\binom{n_1,\dots,n_k}{m_1,\dots,m_l}}(t) = \mathcal{U}_{\rm S}(t)\mathcal{T}_+\Bigg\{ &\int_0^t d\tau_1 \varphi_{{\rm R};n_1}(t-\tau_1)[-i\mathcal{L}_z(\tau_1)] \\ &\times \cdots \int_0^t d\tau_k \varphi_{{\rm R};n_k}(t-\tau_k)[-i\mathcal{L}_z(\tau_k)] \int_0^t d\tau_1' \varphi_{{\rm I};m_1}(t-\tau_1')\mathcal{S}_z(\tau_1') \\ &\times \cdots \int_0^t d\tau_l' \varphi_{{\rm I};m_l}(t-\tau_l')\mathcal{S}_z(\tau_l')\mathcal{U}_{\rm RDM}(t)\Bigg\}\rho_{\rm S}(0).\end{aligned} \tag{A6}$$

Notice that $\mathcal{U}_{\rm RDM}(t)$ cannot be treated as a complete superoperator, since it only denotes an expansion form under the same time-ordering operation with all the other time-dependent superoperators. The order of the hierarchic expansion is determined by $h = k + l$, and the RDM is the zeroth-order dynamic element, $\rho_{\rm S}(t) = \sigma_0(t)$.

Next we take the time derivative over Eq. (A6) to obtain the extended HEOM. For transparency, we organize the time derivative over the t-dependent variables into four different types:

(i) The time derivative of the system time propagator $\mathcal{U}_{\rm S}(t) = \exp(-i\mathcal{L}_{\rm S}t)$ leads to the system Liouville superoperator,

$$\partial_t \mathcal{U}_{\rm S}(t) = -i\mathcal{L}_{\rm S}\exp(-i\mathcal{L}_{\rm S}t) = -i\mathcal{L}_{\rm S}\mathcal{U}_{\rm S}(t). \tag{A7}$$

(ii) The derivative of the time integration is formulated as

$$\begin{aligned}\partial_t \mathcal{T}_+\left\{\cdots\int_0^t d\tau_j \cdots\right\} &\to \varphi_{X;n_j}(0)\mathcal{U}_{\rm S}(t)[-i\mathcal{O}_X(t)]\mathcal{T}_+\left\{\cdots\int_0^t d\tau_{j-1}\int_0^t d\tau_{j+1}\cdots\right\} \\ &= \varphi_{X;n_j}(0)[-i\mathcal{O}_X]\mathcal{U}_{\rm S}(t)\mathcal{T}_+\left\{\cdots\int_0^t d\tau_{j-1}\int_0^t d\tau_{j+1}\cdots\right\},\end{aligned} \tag{A8}$$

with $X = {\rm R,I}$. The superoperator $\mathcal{O}_X$ denotes $\mathcal{L}_z$ ($X = {\rm R}$) and $i\mathcal{S}_z$ ($X = {\rm I}$) accordingly.

(iii) The derivative of the basis set function,

$$\partial_t \mathcal{T}_+\{\cdots\varphi_{X;n_j}(t-\tau_1)\cdots\} = \sum_{j'=1}^{N_X}\eta_{X;j,j'}\mathcal{T}_+\{\cdots\varphi_{X;n_{j'}}(t-\tau_1)\cdots\}, \tag{A9}$$

which is based on the time derivative, $d_t\varphi_{X;j}(t) = \sum_{j'}\eta_{X;j,j'}\varphi(t)$, due to the completeness of $\{\varphi_{X;j}(t)\}$.

(iv) The derivative of the time-ordered integral $\mathcal{U}_{\rm RDM}(t)$ can be organized into

$$\begin{aligned}\partial_t \mathcal{T}_+\{\cdots\mathcal{U}_{\rm RDM}(t)\} = &-i\mathcal{L}_z\sum_{n_{k+1}=1}^{N_{\rm R}} a_{{\rm R};n_{k+1}}\mathcal{T}_+\left\{\cdots\int_0^t d\tau_{k+1}\varphi_{{\rm R};n_{k+1}}(t-\tau_{k+1})[-i\mathcal{L}_z(\tau_{k+1})]\mathcal{U}_{\rm RDM}(t)\right\} \\ &-i\mathcal{L}_z\sum_{m_{l+1}=1}^{N_{\rm I}} a_{{\rm I};m_{l+1}}\mathcal{T}_+\left\{\cdots\int_0^t d\tau_{l+1}'\varphi_{{\rm I};m_{l+1}}(t-\tau_{l+1}')[\mathcal{S}_z(\tau_{l+1}')]\mathcal{U}_{\rm RDM}(t)\right\}.\end{aligned} \tag{A10}$$

As a result, Eqs. (A7)–(A10) allow us to derive the extended HEOM given in Eq. (9) of the main text.

APPENDIX B: THE ASYMPTOTIC EXPRESSION FROM THE GENERALIZED POLARON ANSATZ

In Ref. [8], a generalized polaron ansatz is applied to investigate the delocalized-localized (DL) transition. In the scaling limit of $\omega_c/\Delta \to \infty$, one can derive an analytical expression,

$$\alpha_c = \frac{\sin(\pi s)\exp(-s/2)}{2\pi(1-s)}(2\Delta/\omega_c)^{1-s}, \tag{B1}$$

for the critical Kondo parameter. Notice that an additional prefactor of 2 is included in the tunneling amplitude Δ, due to the difference between our definition of the Hamiltonian and that in Ref. [8]. In the limit of the strong sub-Ohmic bath, $s \to 0$, the Taylor expansion on the spectral exponent s is applied to Eq. (B1), giving an asymptotic form,

$$\alpha_c \sim \frac{1}{2}s\left(\frac{2\Delta}{\omega_c}\right)^{1-s}. \tag{B2}$$

However, the contribution beyond the mean-field approximation may not be ignored, especially when ω_c/Δ is large but finite. One possible way to improve the prediction of Eq. (B2) is to replace the prefactor $1/2$ with a free parameter c. At the end, we obtain

$$\alpha_c \approx cs\left(\frac{2\Delta}{\omega_c}\right)^{1-s}, \tag{B3}$$

which is Eq. (12) in the main text.

[1] A. J. Leggett, S. Chakravarty, A. T. Dorsey, M. P. A. Fisher, A. Greg, and W. Zwerger, Rev. Mod. Phys. **59**, 1 (1987).
[2] S. Sachdev, *Quantum Phase Transition* (Cambridge University Press, Cambridge, 2001).
[3] J. M. Kosterlitz and D. J. Thouless, J. Phys. C **6**, 1181 (1973).
[4] R. Bulla, N.-H. Tong, and M. Vojta, Phys. Rev. Lett. **91**, 170601 (2003).
[5] A. Winter, H. Rieger, M. Vojta, and R. Bulla, Phys. Rev. Lett. **102**, 030601 (2009).
[6] A. Alvermann and H. Fehske, Phys. Rev. Lett. **102**, 150601 (2009).
[7] R. Silbey and R. A. Harris, J. Chem. Phys. **80**, 2615 (1984).
[8] A. W. Chin, J. Prior, S. F. Huelga, and M. B. Plenio, Phys. Rev. Lett. **107**, 160601 (2011).
[9] H. Zheng and Z. Lu, J. Chem. Phys. **138**, 174117 (2013).
[10] Y.-Y. Zhang, Q.-H. Chen, and K.-L. Wang, Phys. Rev. B **81**, 121105 (2010).
[11] D. Z. Xu and J. S. Cao, Front. Phys. **11**, 110308 (2016).
[12] H. B. Wang and M. Thoss, New J. Phys. **10**, 115005 (2008).
[13] H. B. Wang and M. Thoss, Chem. Phys. **370**, 78 (2010).
[14] A. W. Chin, A. Rivas, S. F. Huelga, and M. B. Plenio, J. Math. Phys. (NY) **51**, 092109 (2010).
[15] J. Prior, A. W. Chin, S. F. Huelga, and M. B. Plenio, Phys. Rev. Lett. **105**, 050404 (2010).
[16] C. Guo, A. Weichselbaum, J. von Delft, and M. Vojta, Phys. Rev. Lett. **108**, 160401 (2012).
[17] F. A. Y. N. Schroder and A. W. Chin, Phys. Rev. B **93**, 075105 (2016).
[18] F. B. Anders, R. Bulla, and M. Vojta, Phys. Rev. Lett. **98**, 210402 (2007).
[19] D. Kast and J. Ankerhold, Phys. Rev. Lett. **110**, 010402 (2013).
[20] P. Nalbach and M. Thorwart, Phys. Rev. B **81**, 054308 (2010).
[21] L. Wang, L. P. Chen, N. J. Zhou, and Y. Zhao, J. Chem. Phys. **144**, 024101 (2016).
[22] Y. Tanimura and R. Kubo, J. Phys. Soc. Jpn. **58**, 101 (1989).
[23] Y. Tanimura, J. Chem. Phys. **142**, 144110 (2015).
[24] Y. A. Yan, F. Yang, Y. Liu, and J. S. Shao, Chem. Phys. Lett. **395**, 216 (2004).
[25] A. Ishizaki and Y. Tanimura, J. Phys. Soc. Jpn. **74**, 3131 (2005).
[26] R.-X. Xu, P. Cui, X.-Q. Li, Y. Mo, and Y. J. Yan, J. Chem. Phys. **122**, 041103 (2005).
[27] Y. J. Yan, J. Chem. Phys. **140**, 054105 (2014).
[28] C.-Y. Hsieh and J. S. Cao, arXiv:1701.05709; arXiv:1701.05713.
[29] Y. Tanimura, Phys. Rev. A **41**, 6676 (1990).
[30] C. Meier and D. Tannor, J. Chem. Phys. **111**, 3365 (1999).
[31] J. Hu, R.-X. Xu, and Y. J. Yan, J. Chem. Phys. **133**, 101106 (2010).
[32] H. Liu, L. L. Zhu, S. M. Bai, and Q. Shi, J. Chem. Phys. **140**, 134106 (2014).
[33] Y. Zhou and J. S. Shao, J. Chem. Phys. **128**, 034106 (2008).
[34] J. M. Moix and J. S. Cao, J. Chem. Phys. **139**, 134106 (2013).
[35] Z. F. Tang, X. L. Ouyang, Z. H. Gong, H. B. Wang, and J. L. Wu, J. Chem. Phys. **143**, 224112 (2015).
[36] J. M. Moix, Y. Zhao, and J. S. Cao, Phys. Rev. B **85**, 115412 (2012).
[37] J. Cerrillo and J. S. Cao, Phys. Rev. Lett. **112**, 110401 (2014).
[38] A power-law tail is expected in $k(t)$ for a continuous phase transition. The exponential form of $k^{\rm fit}(t)$ is due to our fitting form of $C(t)$, which is however acceptable since the numerical error induced by the long-time tail $k^{\rm fit}(t)$ is a small number in κ_0.